ELSEVIER

International Journal of Mass Spectrometry 218 (2002) 255–264

International Journal of Mass Spectrometry

www.elsevier.com/locate/ijms

A new accelerator mass spectrometry system for ^{14}C-quantification of biochemical samples

Ted J. Ognibene*, Graham Bench, Tom A. Brown, Graham F. Peaslee[1], John S. Vogel

Lawrence Livermore National Laboratory, Center for Accelerator Mass Spectrometry, L-397, P.O. Box 808, 7000 East Avenue, Livermore, CA 94550, USA

Received 22 January 2002; accepted 28 May 2002

Abstract

A compact accelerator mass spectrometry (AMS) system that meets our requirements for ^{14}C-quantification of biochemical samples is described. The spectrometer occupies approximately 5 m^2 of floor space and can measure >300 samples per day with 3% precision. A long diffuse gas cell is used to destroy interfering molecules and to charge exchange injected negative ions. System sensitivity is <1 amol ^{14}C/mg carbon on milligram-sized samples with a dynamic range that extends over 4 orders magnitude. All components, with the exception of the ion source, are commercially available and the system operates reliably with low maintenance. (Int J Mass Spectrom 218 (2002) 255–264)

Keywords: Accelerator mass spectrometry; Biochemical ^{14}C quantification; Charged-particle beams; Molecular ion dissociation; Charge-exchange

1. Introduction

Accelerator mass spectrometry (AMS) provides carbon isotope ratio quantification at part per quadrillion sensitivity in milligram-sized samples with part per thousand precision. AMS was originally developed for use in the geosciences and archeology as a means to determine radiocarbon ages. AMS has been used in the biosciences to provide highly sensitive ^{14}C-quantification at environmentally relevant doses [1]. Recent conference proceedings [2,3] highlight experiments using ^{14}C, as well as other isotopes of biological significance. However, ^{14}C remains one of the most widely used tracers in biochemical studies of toxicology, nutrition, carcinogenesis, pharmacokinetics and protein quantification [4,5].

The LLNL (Lawrence Livermore National Laboratory) 10 MV spectrometer is one of the most versatile and highest throughput systems presently operating [6], but the exploration of lower acceleration voltages [7,8] for detection of specific isotopes leads to the possibility of spectrometers tailored to particular AMS applications. We assembled and tested a 1 MV spectrometer for biochemical tracing of ^{14}C-labeled compounds based on a low-voltage spectrometer for ^{14}C-dating [9]. We sought a design for a low-cost and low-maintenance system that would be attractive to research and industrial institutions without sacrificing performance criteria established during our decade of experience with biochemical AMS.

* Corresponding author. E-mail: ognibene1@llnl.gov
[1] Permanent address: Department of Chemistry, Hope College, Holland, MI 49423, USA.

1387-3806/02/$ – see front matter
PII S1387-3806(02)00734-0

These criteria include: high throughput of between 10 and 20 samples per hour; reproducibility and accuracy in quantifying ^{14}C at 1–5% precision as determined from multiple measurements; reproducible background count rates equivalent to <1 amol (10^{-18} mol) ^{14}C in a milligram of carbon; and capability for measuring carbon samples as small as 50 μg.

The four criteria are reducible to two design constraints. High throughput and precision require intense ion currents from the samples (>100 μA C^-) that are quantitatively transmitted through the spectrometer without differential isotope loss. This constraint led to the use of the LLNL high-intensity ion source [10] which required careful ion optical coupling to the purchased spectrometer components. Reproducible backgrounds, especially for small samples, require complete destruction of molecular isobars while minimizing ion scattering in the high-energy analysis. These scattered ions are eliminated in typical AMS systems using electric (E/q) and magnetic (m/q) analyses prior to ion counting. Other, self-imposed, requirements included the capacity to select from two ion sources and the opportunity to use singly or doubly charged ions in the high-energy analysis.

Ion charge exchange and molecular isobar destruction is accomplished through ion/gas collisions in a gas "stripper" cell located at the center of the accelerator. In higher energy AMS systems, either thin foils or gas cells are used to create high-charge states. However, in low-energy systems in which low-charge states are preferred, dissociated molecules can recombine after passing through a single thin foil. A long canal filled with a very low density gas guarantees multiple collisions while minimizing energy and angular straggling, however, the overall length of the accelerator increases. The use of two closely spaced thin carbon foils has been proposed as a means to destroy interfering molecular isobars at low-terminal voltages [11]. However, at these energies, the thickening of the carbon foil during ion bombardment, will result in unacceptable losses in ion beam transmission and isotope fractionation. Additionally, at low-ion energies, angular and energy straggling are much worse for foils, which tend to be thicker than the gas pressure required for efficient stripping. The use of a low-density gas eliminates the need for frequent foil changing while still providing for a high-efficiency $C^- \rightarrow C^+$ and $C^- \rightarrow C^{2+}$ charge exchange reactions.

This paper describes the spectrometer and its operation in terms of how well our design constraints delivered the performance needed for biochemical AMS.

2. Experimental

2.1. Description of spectrometer

The spectrometer, shown schematically in Fig. 1, is centered around a National Electrostatic Corporation 3SDH-1 1 MV Pelletron® tandem accelerator. Approximately 300 μA of negative ions are produced from the ion source by cesium ions sputtered onto carbonaceous solid samples (i.e., graphite). These ions are extracted to ground from the 40 kV ion source potential. This ion source is attached to one port of the 45° electrostatic analyzer (ESA) through a 2 einzel lens zoom telescope. The 45° ESA can be rotated to accept ion beams from a second ion source (not shown). Ions are momentum-selected by a 90° double focusing magnetic dipole (injection magnet). Transmitted ions are accelerated by the 520 kV voltage on the initial electrostatic acceleration column. Positive ions resulting from charge exchange reactions with gas molecules are then accelerated through an additional 520 kV and are momentum analyzed by a 90° double focusing dipole magnet (analyzer magnet). A 90° electrostatic spherical analyzer energy-filters the ions before impinging on a 450 mm^2 silicon surface barrier particle detector. The spectrometer is housed in a 44 m^2 room adjacent to and is ∼20% the size of our original spectrometer.

Control of the system operating parameters is maintained using National Instruments Corporation LabView® running on a PC. Custom software selects the sample and controls data acquisition through a CAMAC interface [12].

The high-voltage terminal and charging system of the accelerator are enclosed in a 1.7 m^3 steel tank

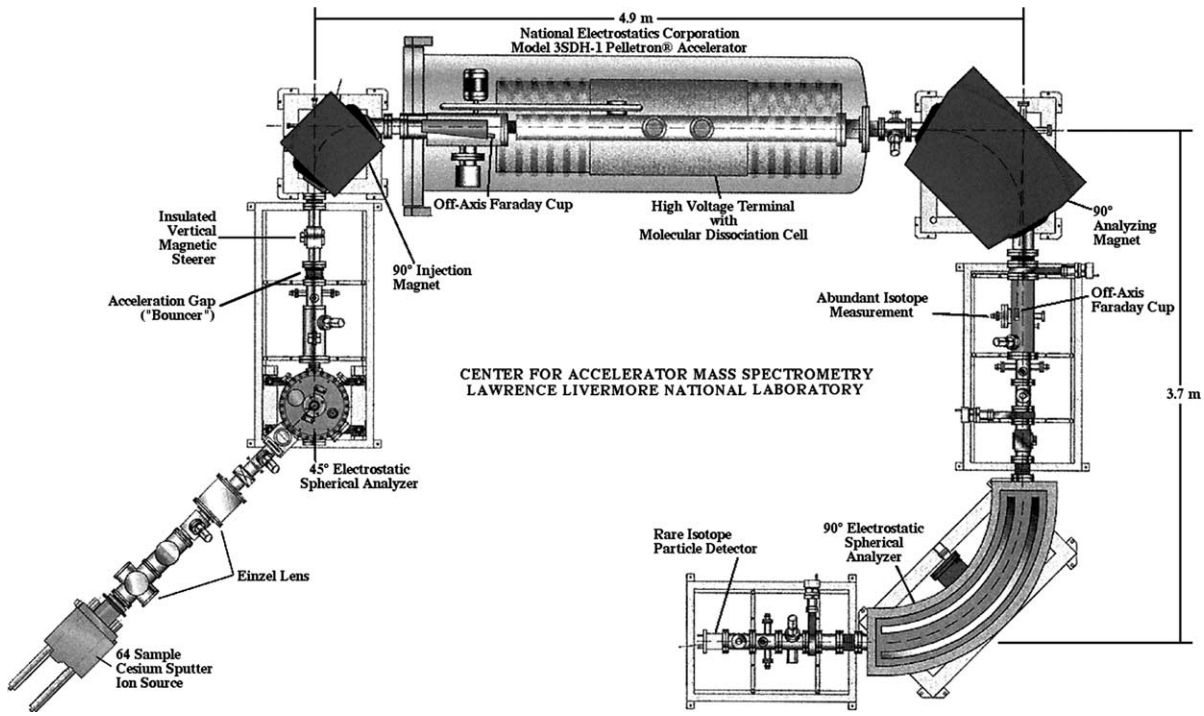

Fig. 1. Schematic layout of the LLNL AMS system for biochemical ^{14}C measurements.

pressurized to 5.62 kg/cm^2 gauge SF_6 insulating gas. An activated alumina filter dries and removes breakdown products from electrical discharges in the gas. A generating voltmeter reads the electrostatic field at the tank wall to determine the terminal voltage (there is no corona feedback in this system). Voltage on the high-potential terminal is stabilized by a feedback system that controls the charging voltage and hence the charging current. Voltage stability to better than 1 kV with $\leq$500 V (FWHM) voltage ripple is achieved.

Before the system was constructed, ion optics modeling was performed to match the emittance of the ion source to the acceptance of the accelerator [13]. The purpose of these calculations was to optimize the layout of the low-energy beam line components so that the large ion currents extracted from the source would be fully exploited to maintain the high sample throughput of our 10 MV system. These calculations were confirmed by ion beam tests of the low-energy injection beam line prior to construction of the higher energy beam line components.

Similar ion optics calculations were performed for the high-energy analysis beam line. The source of the high-energy ion beam was placed at the midpoint of the gas stripper canal. The initial beam spot size was based on the results of optics calculations of the low-energy injection line with an assumed increase of $\sim$20% in the size and divergence in both the radial and vertical planes [14]. The results of these calculations were used to determine the placement of the analyzer magnet, the 90° ESA and the particle detector. Additionally, the optics calculations indicate the location of beam waists for the placement of beam line slits.

During routine operation of the spectrometer, the ion beam is most affected by changes in ion optical components of the low-energy injection beam line. Any isotope-dependent beam focusing at the bouncer gaps is mitigated through the adjustment of the electric fields of the two einzel lenses. Observation of both

the ^{14}C count rate and the ^{13}C current while changing field strengths of the ion optical components show that the beam size is smaller than all apertures.

2.2. Molecular dissociation cell

We characterized the spectrometer to determine the operating conditions, to maximize sample throughput and precision and to minimize background. This work primarily involved exploring the effects of changes in the argon gas pressure within the molecular dissociation cell.

The cell consists of a 10 mm i.d. × 700 mm long tube located within the high-voltage center of the tandem accelerator. Two turbomolecular pumps (Leybold Turbovac 151), running at 75 L/s, recirculate the argon gas escaping from each end back to the middle of the gas canal and decrease ion scatter in the high-energy acceleration tubes. A small amount of argon gas bleeds into the middle of the canal to compensate for any losses to maintain a stable gas density. Argon gas flow is controlled via a remote-controlled bleeder valve. Gas pressure is monitored with a thermocouple ion gauge located between this valve and the center of the canal.

Experiments have shown that at least 2 μg/cm^2 argon gas thickness is required to effectively destroy ion molecules, while significantly less is needed for charge exchange reactions [15]. In the absence of detailed modeling of the gas flows to determine the proper gas thickness, the gas bleed rate into the center of the canal can be adjusted, while the gas pressure is monitored and changes in the ^{14}C detector signal are observed. For a ^{14}C-free carbonaceous sample (i.e., graphitized coal), observed counts in the particle detector with respect to the measured stable ion current, will drop as more molecules are destroyed with increasing gas pressure. The lowest level obtained ultimately determines the sensitivity of the system.

2.3. Isotope ratio measurement

AMS measures isotope ratios: the amount of the rare isotope (^{14}C) is measured with respect to a stable isotope (^{13}C). An electrostatic acceleration gap (“bouncer”) located on either side of the injection magnet is used to rapidly change the energy of the injected ion beam to match the momentum requirements of the injector magnet. Mass-13 ions can then be transmitted through the accelerator, before quantification in an off-axis Faraday cup located at the image plane of the analyzer magnet. In this system, $^{12}C^-$ is measured in an off-axis Faraday cup located inside the SF_6 pressure tank but before the high-voltage terminal and concurrently with the ^{13}C ions.

The carbon isotope ratio is obtained by measuring the rare isotope for 300 ms, followed by a 3 ms stable isotope measurement with small wait times between isotope changes. This cycle is repeated until either the desired ^{14}C counting statistics or the maximum sample measurement time is reached. An electronic pulser is used to calculate counting electronics deadtime from which the isotope ratio is corrected. The isotope concentration of the sample is obtained through comparison to the measurement of similarly prepared standards with a background level subtracted from both [16].

To aid in the characterization of the spectrometer, a variety of standards were used. Although the oxalic acid I standard, with an accepted value of 1.0398 Modern [17], was used for normalization, others include oxalic acid II [18], TIRI Turbidite carbonate [19] and TIRI Belfast pine [19]. The ^{14}C levels of these standards range from 0.1 to 1.3 Modern which span the ^{14}C activity of the majority of biological samples measured by our system. Levels of the carbon concentration in contemporary living creatures are variable, however, the unit Modern is a well-defined number equal to a $^{14}C/C$ isotope ratio of 1.180×10^{-12} which is close to the naturally occurring ^{14}C concentration in the biosphere. This unit is also equivalent to 97.8 amol/mg C and 6.11 fCi/mg C.

2.4. Ion charge state

This spectrometer was designed to measure both $q = +1$ and $q = +2$ carbon ions. However, the

measurement of $^{14}C^{2+}$ is hampered by $^{7}Li^{+}$ ion contamination. Lithium is introduced into the sample during its conversion to graphite and varies from sample to sample [20]. $^{7}Li_2^{-}$ ion molecules are injected into the accelerator along with $^{14}C^{-}$. This often results in the production of two $^{7}Li^{+}$ ions. With the use of silicon surface barrier detectors, coincident detection of these ions does occur and produces a signal indistinguishable to that from a $^{14}C^{2+}$ ion. Without deconvolution of the detector signal, both the sensitivity and accuracy of the system will be adversely affected. The lithium ion contribution can be inferred from the $^{7}Li^{+}$ singles rate. However, this would produce additional error in the ^{14}C quantification. Consequently, we chose to perform ^{14}C measurements of graphite samples in the +1 charge state, which is unaffected by co-injection of the lithium dimer. A CO_2-fed ion source to be installed on the second port of our ESA should not suffer from this background.

3. Results and discussion

3.1. Sensitivity and dynamic range

Fig. 2 shows a plot of carbon isotope ratios measured at different argon gas pressures for graphitized coal samples. In this spectrum, all events falling within the appropriate hardware and software gates are recorded as $^{14}C^{+}$. Each data point represents an average of at least three measurements of three different samples with the error bars indicating the 1-sigma standard deviation about the mean. The average background between 48 and 61 mTorr is 0.0086 Modern (0.84 amol ^{14}C/mg carbon). As the gas pressure increases, ion scattering in the gas canal and beam line tubes increases, which results in the higher background levels observed in the detector. No attempt was made to differentiate sources contributing to detector signal when tuned to ^{14}C. However, one source of background could arise from $^{14}N^{+}$. This ion is present

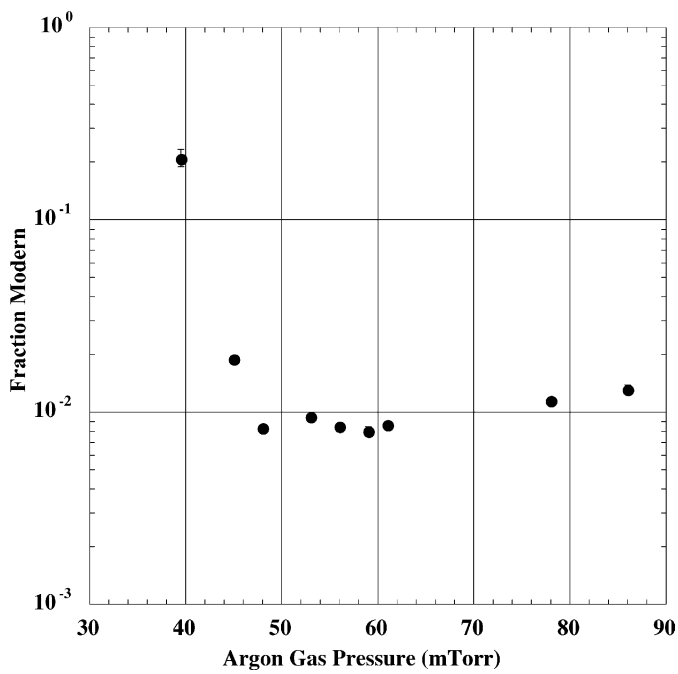

Fig. 2. Carbon isotope ratios measured as a function of argon gas pressure in the molecular dissociation cell. Tandem accelerating voltage of 540 kV was applied during these tests. Error bars, when not shown, are smaller than the data point.

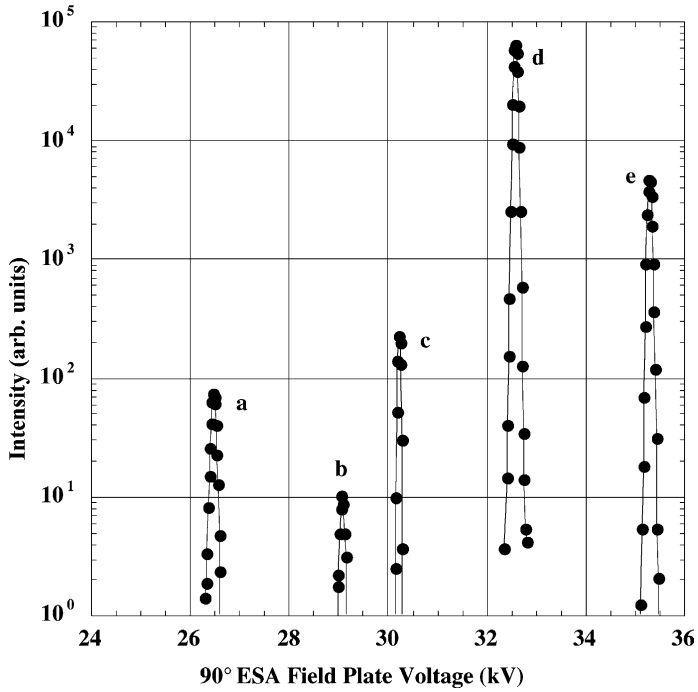

Fig. 3. Detected ion flux, normalized to injected ion current, with respect to voltage applied to the 90° electrostatic spherical analyzer field plates. All other ion optical elements were tuned for ^{14}C transmission with 49 mTorr argon gas stripper pressure. Only significant peaks from 24 to 36 kV were recorded. Peak assignments are presented in Table 1.

from the breakup of $^{14}NH^-$ whose low-energy tail is co-injected into the accelerator with mass = 14 ions. Similarly prepared coal samples are <0.002 Modern when measured on the 10 MV FN tandem indicating that about 3/4 of the counts are still scattered ions or contaminants. No significant changes to the results presented in Fig. 2 were observed with changes in the tandem accelerating voltage.

The upper limit of $^{14}C^+$ quantification arises from memory effects in the ion source, which prevent rapid sample sequencing for samples with carbon ratios >1000 Modern. However, the upper quantifiable limit is set at 400 Modern by detector electronics deadtime during which the silicon surface barrier particle detector cannot distinguish individual particles. The use of an electron multiplier to increase this upper limit is being explored [21]. In the mean time, the upper limit can be extended through dilution of the source material.

3.2. Background ions

Fig. 3 shows a scan of the field plates of the 90° electrostatic analyzer (ESA) with total counts recorded by the silicon particle detector of a graphitized oxalic acid I standard. All other ion optical elements were set to transmit ^{14}C through the system. The detector signal was normalized to the ion current measured with the off-axis Faraday cup located before the tandem accelerator. While only the significant peaks were recorded in detail, there is a small background throughout the entire spectrum.

The peak assignments are presented in Table 1. The peak at 30.2 kV can be definitively assigned to $^{14}C^+$. A similar scan of a ^{14}C-free graphite[2] shows a similar spectrum with the exception of the peak at

[2] Alfa Aesar Stock # 14734, graphite powder, −200 mesh, 99.9999% purity.

Table 1
Peak assignments for Fig. 3

Peak	Voltage (kV)	Assignment
a	26.5	Scattered $^{16}O^+$ (tentative)
b	29.1	$^{13}C^+$ from ^{13}CH breakup
c	30.2	$^{14}C^+$
d	32.6	Scattered $^{13}C^+$
e	35.3	Scattered $^{12}C^+$

30.2 kV. Based on kinematics, the peak at 29.1 kV can be assigned to $^{13}C^+$, from the breakup of the $^{13}CH^-$ molecule which is co-injected with $^{14}C^-$ into the accelerator. The peaks at 32.6 and 35.3 kV, respectively, result from $^{13}C^+$ and $^{12}C^+$ scatter and have the correct energy to have been transmitted along with the full-energy $^{14}C^+$ ions through the analyzer magnet. A similar argument can be made for the tentative assignment of the peak at 26.5 kV to $^{16}O^+$. The cesium sputter source generates copious oxygen beams [22], whose low-energy tail is co-injected with $^{14}C^-$ into the accelerator. After charge exchange and subsequent acceleration, the analyzer magnet selects a single momentum to be transported to the 90° ESA.

Given that $^{13}C^+$ from the dissociation of ^{13}CH is observed, we would expect to detect $^{12}C^+$ from the breakup of the $^{12}CH_2$ molecule. Evidence of this breakup would result in a peak around 28 kV. However, this molecule is present at approximately 1/10 the intensity of the ^{13}CH molecule [15]. Hence, any peak from $^{12}CH_2$ breakup would be indistinguishable from the background in our system.

The full-width half-maximum (FWHM) energy resolution of the 90° ESA is calculated to be approximately $1100E/\Delta E$ from the ^{14}C peak in Fig. 3.

All of the peaks in Fig. 3 have energy tails associated with them that can interfere with the $^{14}C^+$ signal. The low energy of the ions makes the use of particle identification through dE/dx techniques problematic. Additional ion optical elements such as a magnet or a velocity filter would remove a significant fraction of these tails. However, this would increase the size, complexity and cost of the AMS system. A reduction

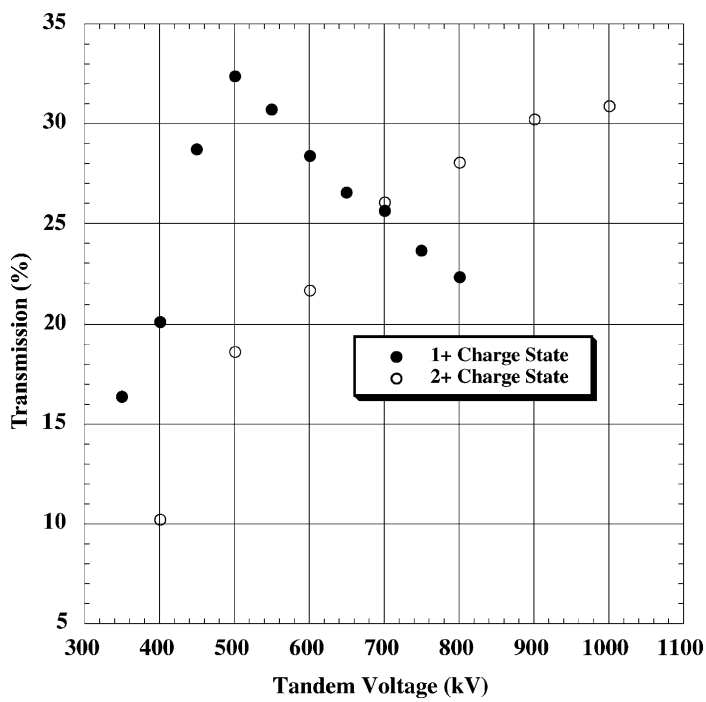

Fig. 4. Carbon ion transmission through the accelerator with respect to accelerating voltage. See text for details.

in scattered ions would be achieved through a redesign of the stripper canal, with improved vacuum pumping. The new generation of sub 1 MV tandem accelerators from National Electrostatics Corporation uses shorter stripper canals with larger diameters, as well as faster turbomolecular vacuum pumps. A background of 0.0026 Modern has been observed from processed coal samples [23].

3.3. Ion transmission

Fig. 4 shows the carbon transmission through the accelerator as a function of accelerating voltage for both the +1 and +2 charge states at an argon gas pressure of 50 mTorr. Transmission was calculated by measuring the $^{12}C^-$ current in the off-axis Faraday cup before the accelerator. The ^{12}C signal was scaled to ^{13}C assuming a 1.11% $^{13}C/^{12}C$ isotope ratio and compared to the measured ^{13}C ion current measured in an off-axis Faraday cup at the analyzer magnet image plane after the accelerator. Direct measurement of the $^{13}C^-$ current before the accelerator is not possible due to $^{12}C^-$ molecular ion interference. The $^{12}CH^-$ ion beam is too intense to inject into the accelerator without drawing the accelerating voltage down.

At acceleration voltages below 400 kV, the ion transmission is dominated by ion scattering losses which decrease as the ion velocities increase. At a constant stripper pressure, measured $q = +1$ carbon ion transmission drops at the high-tandem voltage because the cross section for the charge exchange reaction is dropping. These two conditions result in a peak in ion transmission around 520 kV for the +1 charge state. With better than 1 kV control, we

Table 2
Summary results for a series of standards, analyzed as unknowns on the 1-MV AMS spectrometer. Results are compared to the accepted values

Sample name	Identification number	Measured value (Fraction modern)	Accepted value (Fraction modern)	Difference (part per 1000, ‰)
TIRI Turbidite	37852	0.1034 ± 0.0037		
TIRI Turbidite	37854	0.1027 ± 0.0037		
TIRI Turbidite	37853	0.1047 ± 0.0037		
Average		0.1036 ± 0.0010	0.1043[a]	6.7
TIRI Wood	37173-31	0.5696 ± 0.0029		
TIRI Wood	35359-32	0.5747 ± 0.0027		
TIRI Wood	35359-28	0.5680 ± 0.0026		
Average		0.5708 ± 0.0035	0.5709[b]	0.2
Oxalic acid I	37463-5	1.0457 ± 0.0042		
Oxalic acid I	37527-26	1.0305 ± 0.0075		
Oxalic acid I	37527-27	1.0358 ± 0.0037		
Oxalic acid I	37527-24	1.0360 ± 0.0037		
Oxalic acid I	37522-31	1.0403 ± 0.0037		
Average		1.0376 ± 0.0057	1.0398[c]	2.1
Oxalic acid II	36452-11	1.3349 ± 0.0032		
Oxalic acid II	36452-10	1.3415 ± 0.0030		
Oxalic acid II	37528-9	1.3425 ± 0.0032		
Average		1.3396 ± 0.0041	1.3407[d]	0.8

[a] Turbidite carbonate, TIRI sample K consensus value [19].
[b] Belfast pine, TIRI sample B consensus value [19].
[c] HoxI [17].
[d] HoxII, National Institute of Standards and Technology, designation SRM 4990C [18].

can set the terminal voltage 520 kV to maximize ion transmission during routine sample analysis. The data suggests that the peak of the +2 charge state carbon ion transmission has been reached at around 1000 kV.

Measurements at ETH in Zurich show that there is a broad maximum in the charge exchange cross section with ~50% of the C^- ions converted to C^+ between 200 and 600 keV [15]. The data shown in Fig. 4 does not reflect this, as no attempt was made to unfold losses due to ion scattering which can be quite significant at these energies [14]. There are no ion beam transmission losses from the analyzer magnet focal plane to the ^{14}C particle detector.

During these tests, only the analyzer magnet field was tuned for maximum ion transmission when the accelerating voltage was changed. It is possible that the ion source extraction voltage must be adjusted with large changes to the accelerating voltage to achieve optimal coupling between the accelerator and the ion beam phase space. However, this ion source is designed to extract ions at 40 kV. Extraction at higher potentials might necessitate changes to insulating gaps. Lowering the ion source extraction voltage would decrease the source output and thus adversely affect sample throughput.

3.4. Accuracy and precision

Measurements of known standards are presented in Table 2. Each measurement represents either 15,000 ^{14}C counts or 45 s analysis time. Typical $^{13}C^+$ ion currents were 600 nA. Each measurement was normalized to an average of five measurements of graphitized oxalic acid I. Agreement between the measured averages and the accepted fraction modern value for each standard is excellent as indicated in the last column of Table 2. The precision in each measurement for all but the TIRI Turbidites is also excellent, averaging approximately 6‰. The larger average precision of 1.0% on the TIRI Turbidite measurements mainly arises from increased counting error from fewer events. The largest source of error in each measurement results from the large relative uncertainty in the subtracted background value.

Table 3
Summary performance and operating parameters for the 1-MV spectrometer

Sample performance	
Sensitivity	<0.01 Modern (<1 amol ^{14}C/mg carbon)
Dynamic range	4–5 orders of magnitude
Sample throughput	100 samples/8 h (average)
Precision	3%
Operation	
Ion source	64 sample cesium sputter
Extraction voltage	40 kV
Source output	300 μA (typical)
Injector magnet resolution	$130M/\Delta M$
Analyzed low-energy ions	40 keV $^{12}C^-$ (170 μA typical)
Accelerator voltage	520 kV
Ion stripping gas pressure	~50 mTorr argon
Analyzer magnet resolution	$250M/\Delta M$
90° ESA resolution	$1100E/\Delta E$
Analyzed stable ions	1.08 MeV $^{13}C^+$ (600 nA typical)
Analyzed rare ions	1.08 MeV $^{14}C^+$

4. Conclusions

Routine operation of the spectrometer for biochemical ^{14}C measurements began in April 2001. Since then, over 4000 samples have been measured. We are also using this spectrometer to explore other isotopes and for development of AMS methods when it is not busy with routine measurements. Table 3 provides a summary of relevant performance and operation parameters. This performance is nearly identical to that obtained when biochemical samples are analyzed using the 10 MV accelerator.

Acknowledgements

This work was performed under the auspices of the U.S. Department of Energy by University of California, Lawrence Livermore National Laboratory under contract no. W-7405-Eng-48 and under the National Center for Research Resources Grant no. RR13461. The authors wish to acknowledge John Southon for many useful discussions and insights. Dan Espinosa, Skip Fields, Dallas Gittins, Randy Leber and Joe Ruth are recognized for their efforts during construction.

Brian Frantz is also acknowledged for the preparation of many of the samples used in the testing of the spectrometer.

References

[1] S.P.H.T. Freeman, J.S. Vogel, Int. J. Mass Spectrom. 143 (1995) 247.
[2] A.J.T. Jull, J.W. Beck, G.S. Burr (Eds.), Proceedings of the Seventh International Conference on Accelerator Mass Spectrometry, Nucl. Instr. Meth. B 123 (1997) 1.
[3] W. Kutschera, R. Gloser, A. Priller, B. Strohmaier (Eds.), Proceedings of the Eighth International Conference on Accelerator Mass Spectrometry, Nucl. Instr. Meth. B 172 (2000) 1.
[4] K.W. Turteltaub, J.S. Vogel, Curr. Pharm. Des. 6 (2000) 991.
[5] M. Miyahita, J.M. Presley, B.A. Buchholz, K.S. Lam, Y.M. Lee, J.S. Vogel, B.D. Hammock, Proc. Natl. Acad. Sci., U.S.A. 98 (2001) 4403.
[6] M.L. Roberts, G.S. Bench, T.A. Brown, M.W. Caffee, R.C. Finkel, S.P.H.T. Freeman, L.J. Hainsworth, M. Kashgarian, J.E. McAninch, I.D. Proctor, J.S. Southon, J.S. Vogel, Nucl. Instr. Meth. B 123 (1997) 57.
[7] H.W. Lee, A. Galindo-Uribarri, K.H. Chang, L.R. Kilius, T.E. Litherland, Nucl. Instr. Meth. B 5 (1984) 208.
[8] M. Suter, St. Jacob, H.A. Synal, Nucl. Instr. Meth. B 123 (1997) 148.
[9] H.-A. Synal, S. Jacob, M. Suter, Nucl. Instr. Meth. B 172 (2000) 1.
[10] J.R. Southon, M.L. Roberts, Nucl. Instr. Meth. B 172 (2000) 257.
[11] B.J. Hughey, R.E. Shefer, R.E. Klinkowstein, X.L. Zhao, W.E. Kieser, A.E. Litherland, Nucl. Instr. Meth. B 123 (1997) 186.
[12] A. Berno, J.S. Vogel, M. Caffee, Nucl. Instr. Meth. B 56 (1991) 1076.
[13] T.J. Ognibene, T.A. Brown, J.P. Knezovich, M.L. Roberts, J.R. Southon, J.S. Vogel, Nucl. Instr. Meth. B 172 (2000) 47.
[14] P. Sigmund, K.B. Winterbon, Nucl. Instr. Meth. B 119 (1974) 541.
[15] S.A.W. Jacob, M. Suter, H.A. Synal, Nucl. Instr. Meth. B 172 (2000) 235.
[16] T.A. Brown, J.R. Southon, Nucl. Instr. Meth. B 123 (1997) 208.
[17] National Institute of Standards and Technology, Gaithersburg, MD, designation SRM 4990.
[18] W.B. Mann, Radiocarbon 25 (1983) 519.
[19] M. Scott, D. Harkness, G. Cook, Report on Third International Radiocarbon Intercomparison, 1997, unpublished.
[20] D.H. Loyd, J.S. Vogel, S. Trumbore, Radiocarbon 33 (1991) 297.
[21] K. Yuasa-Nakagawa, S.-M. Lee, T. Nakagawa, I. Tanihata, Nucl. Instr. Meth. A 300 (1991) 538.
[22] R. Middleton, A Negative Ion Cookbook, 1889, unpublished.
[23] National Electrostatics Corporation, Personal communication, 2000.